Morphologies of Microphase-Separated A_2B Simple Graft Copolymers

Darrin J. Pochan and Samuel P. Gido*

Department of Polymer Science and Engineering, University of Massachusetts−Amherst, Amherst, Massachusetts 01003

Stergios Pispas and Jimmy W. Mays

Department of Chemistry, University of Alabama−Birmingham, Birmingham, Alabama 35294

Anthony J. Ryan,[†,‡] J. Patrick A. Fairclough,[‡] Ian W. Hamley,[§] and Nicholas J. Terrill[‡]

CLRC Daresbury Laboratory, Warrington, WA4 4AD U.K., Materials Science Centre, UMIST, Grosvenor Street, Manchester, M1 7HS U.K., and School of Chemistry, University of Leeds, Leeds, W. Yorkshire, LS2 9JT U.K.

Received November 14, 1995; Revised Manuscript Received May 7, 1996[⊗]

ABSTRACT: The morphological behavior of a series of well-defined A_2B simple graft or "Y" architecture block copolymers is characterized via small-angle X-ray scattering (SAXS) and transmission electron microscopy (TEM). This model architecture is formed by grafting a polystyrene block onto the center of a polyisoprene backbone. The volume fraction windows in which specific strongly segregated microphase-separated morphologies are observed are shifted to higher volume fractions of the PS graft material than in the corresponding linear diblock copolymers. These findings are in good agreement with recently calculated theoretical phase behavior for simple graft, A_2B, block copolymers. However, a new morphology, not found in neat linear diblock copolymers, is also observed. This A_2B material is microphase separated into wormlike micelles but not ordered on a lattice. This morphology is found at high PS graft volume fraction ($\phi_s = 0.81$), where the two PI chains per molecule are initially forced to the concave side of the PS/PI interface.

1. Introduction

For linear diblock copolymers in the strong segregation limit (large χN), the morphology formed is solely dictated by the relative volume fractions of the respective blocks. Changing molecular architecture, making graft block copolymers for instance, can allow control of the morphology independent of the volume fraction, thus providing an additional variable for control of structure. A_2B simple graft block copolymers (Figure 1) are systems in which strong segregation limit (SSL) microphase-separated morphologies are expected to occur in volume fraction ranges which are higher in the B block than for AB linear diblocks. These simple graft block copolymers are models for more complex multiple graft block copolymers typically used as compatibilizing and toughening agents in polymer blends. In the work reported here, a polystyrene (PS) block is utilized as the graft chain while polyisoprene (PI) forms the backbone in a range of relative volume fractions.

In the SSL, the interphase region between domains has been measured and theoretically modeled to be only about 20−50 Å.[1−3] By comparison, to the length scale of the microphase-separated domains, typically hundreds of angstroms, the interphase region can be considered a two-dimensional surface. This interface, which has been called an intermaterial dividing surface,[4] has curvature properties which can be approximately correlated to the volume-filling characteristics of the opposing blocks of the copolymer. The volume available to a polymer chain increases as one moves from the concave to the convex side of a curved interface in a block copolymer, and the disparity in the relative volumes available to the two blocks is proportional to the magnitude of the interfacial curvature. Thus the highest curvature interface geometry, spheres, occurs for the most asymmetric block volume fractions. As the volume fraction difference decreases, so does the interfacial curvature across the sequence of observed morphologies: spheres, cylinders, cubic bicontinuous, and lamellar. As illustrated in Figure 1, an A_2B graft architecture will greatly alter the chain packing of the two block materials on the two sides of the interface. The two A chains are more highly stretched and experience more lateral crowding than the single B chain. Therefore, the A phase will favor the convex side of the interface at volume fractions (ϕ_A from about 0.34 to 0.50) where a simple AB diblock would prefer a flat, lamellar interface.

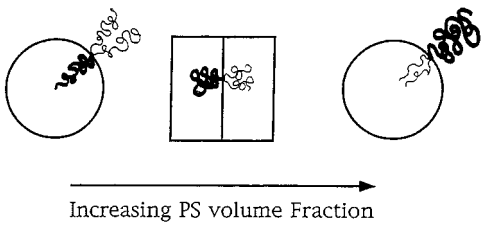

Figure 1. Schematic of the A_2B, or "Y", molecular architecture in the microphase-separated state. The two A chains per molecule are calculated[5] to reside on the convex side of a curved A/B interface until much higher volume fractions than what is experimentally found in diblock architecture.[27] A curved A/B interface generically represents spherical, cylindrical, and bicontinuous morphologies while the flat interface represents a lamellar morphology.

* To whom correspondence should be addressed.
† CLRC Daresbury Laboratory.
‡ UMIST.
§ University of Leeds.
⊗ Abstract published in *Advance ACS Abstracts,* June 15, 1996.

S0024-9297(95)01696-2 CCC: $12.00

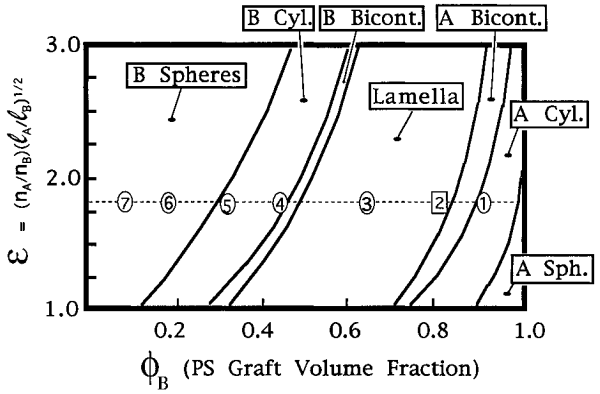

Figure 2. Theoretical phase diagram calculated by Milner.[5] The ovals along the dashed line where $\epsilon = 1.78$ each represent a specific I_2S sample corresponding to the number within the oval. I_2S-2 is represented by a square due to its unusual morphology not found in linear diblocks or accounted for theoretically in this phase diagram.

The SSL behavior of simple graft architecture studied in this paper was recently explored in the mean-field calculations of Milner[5] and the ground-breaking synthesis and subsequent initial morphological studies of Hadjichristidis.[6] Both works reveal intriguing results introduced by the simplest case of an architectural asymmetry in the form of an A_2B simple graft or "Y" block copolymer. As a way to reveal bulk morphological effects of grafting the chains in this manner, Milner used a simple calculation to reveal the center of the lamellar phase in a melt of "Y" polymers. It was found that the B graft component volume fraction is $\phi_B = {}^2/_3$ in an A_2B graft block copolymer to produce a flat preferred interfacial curvature. The analogous absence of a preferred curvature for symmetric diblock architecture occurs at $\phi_B = {}^1/_2$ revealing the shift of the center of the phase diagram due to architecture alone. The possible morphologies were modeled with round unit cells for the cylindrical and spherical phases and utilized an approximation based on "Gaussian wedges"[7] to describe a generic bicontinuous phase. The morphology phase diagram was calculated by minimizing the sums of the free energies associated with the interfacial tension between phases and the stretching of the blocks away from the interface. The latter was calculated with methods developed for polymer brushes.[8] The crossings of the free energy curves for the differing geometries vs graft volume fraction determine the equilibrium SSL phase behavior as shown in Figure 2. The diagram is generic in that within the parameter $\epsilon = (n_a/n_b)(l_a/l_b)^{1/2}$ different architectures and chain statistics are accounted for. The number of arms one chooses, n_a of A or n_b of B, can be varied. Also, differing chain statistics between blocks are represented in the square root ratios of l_a and l_b with $l_i = V_i/R_i^2 = v_i/b_i^2$, where V_i and R_i are the molecular volume and radius of gyration of the respective blocks and v_i and b_i are the segment volume and Kuhn length of the respective blocks. If the constituent blocks are conformationally symmetric, then ϵ is simply the ratio of the number of A and B arms in the molecule.

At $\epsilon = 1$ the phase diagram models linear, AB diblock phase behavior, with the phases being symmetric around $\phi_b = 0.5$. However, as one increases arm number of one species relative to the other or varies the relative chain statistics of A and B, the phase behavior becomes extremely asymmetric with volume fraction. Hadjichristidis *et al.*[6] recently characterized the bulk phase behavior of three A_2B block copolymers or "miktoarm" star copolymers. The asymmetry of the graft architecture forced two of their samples to shift the observed morphology away from that which would be formed by diblock architecture analogs with the same component volume fractions: A 37 vol % polystyrene "I_2S" graft (polyisoprene backbone and a single polystyrene graft emanating from the middle of that backbone) and a 40 vol % styrene SIB graft (the rubbery phase consists of mixed isoprene and butadiene blocks) were observed to form cylindrical phases where diblocks of the same compositions would be bicontinuous or lamellar, respectively. The I_2S blocks studied in this work confirm the strong asymmetry in the phase behavior vs volume fraction for $\epsilon > 1$ shown in Figure 2. However, in addition to simply shifting the volume fractions at which the standard diblock phases are found, the architecture also introduces a novel morphological behavior unique to the simple graft architecture. A new phase is observed at a volume fraction at which the two PI arms per molecule are first forced to the concave side of the PS/PI interface in the microphase-separated state. This phase consists of microphase-separated wormlike micelles which are not ordered on a lattice. A wormlike micelle phase has been previously observed in blends of diblock copolymers with homopolymers,[9] but, to our knowledge, this phase has not been previously observed in neat block copolymers.

2. Experimental Section

I_2S simple graft block copolymers were prepared under high-vacuum conditions in all-glass reactors which had been washed with *n*-BuLi and rinsed with solvent. Additions of reagents were made through breakseals and removals of samples were made through heat sealing of constrictions. The benzene solvent, styrene-d_8 (Cambridge Isotopes, halogen free) and isoprene monomers, CH_3SiCl_3 linking agent, and CH_3OH terminating agent were purified using standard anionic polymerization techniques.[10,11] *s*-BuLi, purified by sublimation under high vacuum, was used as the initiator throughout the synthesis. The reaction scheme followed for the preparation of the $(PI)_2PS$-d_8 miktoarm stars can be represented by the following reactions:[12,13]

$$(PS\text{-}d_8)Li + \text{excess } CH_3SiCl_3 \rightarrow (PS\text{-}d_8)SiCH_3Cl_2 + LiCl + CH_3SiCl_3\uparrow$$

$$(PS\text{-}d_8)SiCH_3Cl_2 + \text{excess } PILi \rightarrow (PI)_2SiCH_3(PS\text{-}d_8) + 2LiCl$$

In the first step, a dilute solution of the living polystyrene-d_8 (d_8 labeling of the PS graft in this work was used to facilitate subsequent analysis of these materials via neutron scattering techniques) was added into a large excess of methyltrichlorosilane (SiCl/Li = 100). Excess methyltrichlorosilane was removed by continuous pumping on the vacuum line followed by redisolution of the polymer with purified benzene and removal of the solvent. This process was repeated twice. In the second step, excess living polyisoprene chains were added to the macromolecular linking agent. When the coupling of the polyisoprene chains was completed, excess polyisoprenyllithium was deactivated with degassed methanol.

Fractionation of the samples was performed by addition of methanol to a 1% solution of the polymers in a 60/40 volume benzene/hexane mixture. Usually three fractionations were enough to remove any unlinked polyisoprene arms. All stages of polymer synthesis were monitored by size exclusion chromatography (SEC). A Waters Model 510 pump, Model 410 differential refractometer, and a LDC/Milton Roy variable-wavelength UV detector in series with three Waters Ultrastyragel linear columns were used. Tetrahydrofuran was

Table 1. I_2S Molecular Characteristics

sample	vol % d-PS[f]	M_n(PS arm)[a] ($\times 10^{-3}$)	M_n(PI arm)[a] ($\times 10^{-3}$)	M_n(total)[a] ($\times 10^{-3}$)	A_2[a] ((mol mL)/g^2) ($\times 10^3$)	M_w/M_n[b]	M_w(total)[c] ($\times 10^{-3}$)	A_2[c] ((mol mL)/g^2)	wt % d-PS[d]
I_2S-1	89	87.3	4.6[e]	97.1	0.50	1.04	106.0	0.56	91
I_2S-2	81	79.1	9.6	89.4	0.61	1.04	90.8	0.57	84
I_2S-3	62	61.2	14.8	83.0	0.65	1.04	87.4	0.80	67
I_2S-4	44	44.4	21.3	82.5	0.77	1.04	92.0	0.76	49
I_2S-5	31	31.6	26.5	82.6	1.02	1.04	89.8	0.83	35
I_2S-6	17	21.1	34.7	92.3	1.10	1.04	100.1	1.06	20
I_2S-7	8	9.4[e]	39.1	84.3	1.03	1.06	91.3	1.10	10

[a] By membrane osmometry. [b] By SEC. [c] By LALLS. [d] By SEC−UV. [e] By VPO. [f] Calculated utilizing $\rho(d\text{-PS}) = 1.14$ g/mL^3 at 25 °C and $\rho(\text{PI}) = 0.91$ g/mL^3 at 25 °C along with the weight percent compositions from SEC−UV.

the elution solvent at a flow rate of 1 mL/min at 35 °C. Composition of the samples was measured by SEC−UV at 260 nm after calibration with several concentrations of polystyrene standards.

Number-average molecular weights (M_n) and second virial coefficients (A_2) for the copolymers and the arms were determined with a Wescan Model 231 membrane osmometer at 37 °C. RC-51 membranes were used with CaH_2 distilled toluene as the solvent. In all cases, M_n and A_2 values were obtained from the $(\pi/c)^{1/2}$ vs c plots, where π is the osmotic pressure and c is the concentration. For molecular weights lower than 10 000 a UIC Model 070 vapor pressure osmometer was used. HPLC grade benzene was the solvent at 40 °C. The instrument was calibrated with benzil.

As an additional check, apparent weight-average molecular weights (M_w) and A_2 for the copolymers were measured with a Chromatix KMX-6 low-angle laser light scattering photometer equipped with a helium−neon laser. The M_w values were obtained from $(Kc/\Delta R_0)^{1/2}$ vs c plots, where ΔR_0 is the excess Rayleigh ratio, c is the concentration, and K is a combination of known optical constants including the refractive index increments dn/dc. Values of dn/dc were also measured in THF at 25 °C with an Otsuka DRM-1020 differential refractometer at 633 nm calibrated with NaCl solutions. Within experimental uncertainty the light scattering data are consistent with results from membrane osmometry. The molecular characteristics of the samples are given in Table 1.

Solid films approximately 2 mm thick were cast from toluene solutions of 5 wt % polymer in 30 mL Pyrex beakers. The evaporation of solvent was controlled to form a solid film after 10−14 days. The films were given several more days at room temperature and atmospheric pressure and an additional several days under high vacuum at room temperature to allow residual solvent to evaporate. The vacuum oven temperature was ramped to 120 °C over a period of 3 days and kept there for 1 week. After annealing, the temperature was slowly ramped down to 80 °C over 2 days and then quickly lowered to room temperature. This casting and annealing procedure was designed to promote the development of equilibrium strong segregation morphologies. After the oven temperature exceeded approximately 110 °C, sample I_2S-7 began to creep, indicating a loss of microphase-separated order at the order−disorder transition (ODT). A second film of I_2S-7 was annealed at 108 °C, below the ODT of the system but high enough for significant annealing.[15,16]

All samples for electron microscopy were microtomed in a Reichert-Jung cryoultramicrotome. Sections approximately 300−800 Å thick were cut with a Diatome cryo diamond knife at a sample temperature of −110 °C and a knife temperature of −90 °C. The sections were stained in 4 wt % aqueous OsO_4 vapors for 4 h. Transmission electron microscopy experiments (TEM) were performed on a JEOL 100CX electron microscope operated at 100 kV accelerating voltage.

Synchrotron SAXS experiments were performed on beamline 2.1 of the Synchrotron Radiation Source (SRS) at the Daresbury Laboratory, Warrington, U.K. Details of the electron storage ring, radiation, camera geometry, and data collection electronics have been given elsewhere.[17] White radiation from the electron ring was collimated using a cylindrically bent Ge(111) crystal to isolate an intense beam of $\lambda = 1.50 \pm 0.01$ Å X-rays. At 2 GeV and 200 mA the SRS generates a flux of 4×10^{10} photons s^{-1} at the sample/focal plane. The instrument is equipped with a 20 × 20 cm area detector 5 m from the sample position with a vacuum chamber placed in between to reduce air scattering and absorption. The spatial resolution of the detector is 500 μm, and it has a count rate limit of 500 kHz. The bulk polymer films were mounted in the beam after being sandwiched between two pieces of Kapton (polyimide) tape in a desired orientation. An oriented specimen of wet collagen (rat tail tendon) was used to calibrate the SAXS detector. A parallel-plate ionization detector placed before the sample cell recorded the incident intensities. The experimental data were corrected for Kapton and camera background scattering, sample absorption, and the positional alinearity of the detector.

Birefringence observations were performed on bulk films at room temperature with a Leitz optical microscope under cross polars.

3. Results and Discussion

For the sake of comparison with the calculated phase behavior of the simple graft architecture, an approximate ϵ, as described in the Introduction, is assigned to the I_2S system. If PS and PI blocks were conformationally symmetric, then ϵ would simply be the ratio of PI arms to PS or $\epsilon = 2$. However, the slight asymmetry inherent in the different chemical species slightly lowers the ϵ parameter. We assign segmental volumes, v_i, as 132 and 176 Å^3 for PI and PS, respectively.[18] Statistical segment lengths, b_i, are assigned as 6.8 and 6.9 Å for PI and PS, respectively.[19] These values produce an ϵ of 1.78. While these values were measured at different temperatures (123 °C for the segment volumes and 150 °C for the segment lengths), they are adequate in revealing the slight effect the small conformational asymmetry between PS and PI has within the framework of the theoretical phase diagram. Any changes in the values due to temperature or isotope effects would have only a slight effect on ϵ and are accounted for via the size of the symbols on the phase diagram in Figure 2.

Table 2 contains tabulated d-spacings and birefringence information as well as the resulting morphology assignments as described in the remainder of the paper. Birefringence observations were performed on the annealed films as a preliminary measure of the degree of microphase separation. The form birefringence, a result of noncubic symmetry, is evidence of either a cylindrical or a lamellar microstructure.[20,21] The most fundamental facet to this work is the confirmation of asymmetry in the phase behavior vs volume fraction in the simple graft block copolymer architectures. For the simple graft architecture, each particular morphology (spheres, cylinders, lamella, etc.) occurs at a higher PS graft volume fraction than would be expected in a simple diblock architecture. This results in a morphology

Table 2. I_2S Morphology Characteristics

sample	ϕ_s	d_1[a] (Å)	morphology	optical birefringence
I_2S-1	0.89	310 ± 5	hexagonally packed PI cylinders in PS matrix	yes
I_2S-2	0.81	NA	disordered PI micelles	no
I_2S-3	0.62	390 ± 5	alternating PS and PI lamellae	yes
I_2S-4	0.44	429 ± 5	hexagonally packed PS cylinders in PI matrix	yes
I_2S-5	0.31	380 ± 5	hexagonally packed PS cylinders in PI matrix	yes
I_2S-6	0.17	289 ± 5	cubic array PS spheres in PI matrix	no
I_2S-7	0.08	235 ± 5	cubic array PS spheres in PI matrix	no

[a] $d_1 = 2\pi/q_1$, where $q_1 = 4\pi/\lambda(\sin\theta_1)$ and $2\theta_1$ is the scattering angle for the lowest angle Bragg peak; corresponds to $d_{(10)}$ for hexagonally packed cylinders, $d_{(001)}$ for lamellae, and either $d_{(100)}$ or $d_{(110)}$ for simple cubic or body-centered cubic, respectively.

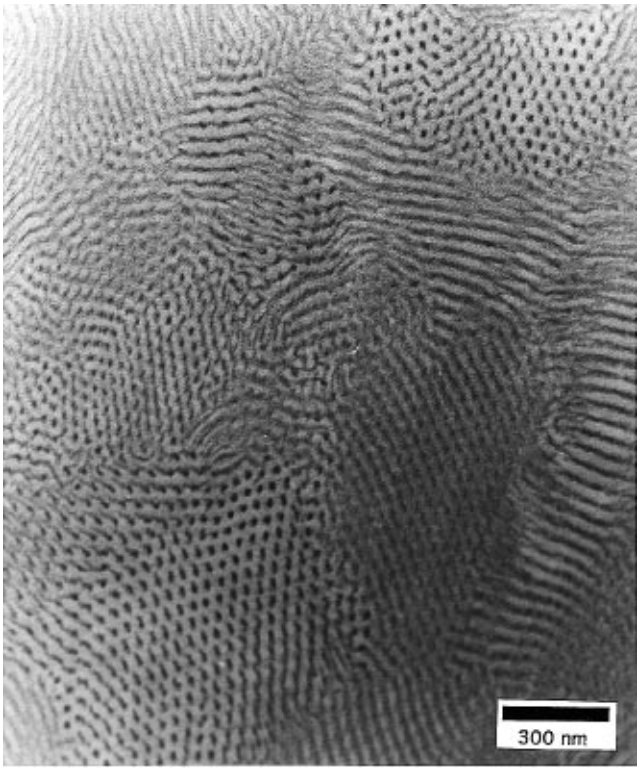

Figure 3. TEM micrograph of I_2S-1 ($\phi_s = 0.89$) showing projections both parallel and perpendicular to the PI cylinders as well as revealing a small average grain size.

diagram which is asymmetric about 0.5 volume fraction and which is in good qualitative agreement with the calculations of Milner.[5] However, in addition to simply shifting normal diblock phase behavior to higher PS volume fractions, the A_2B simple graft architecture also introduces a new morphology in sample I_2S-2 not yet anticipated theoretically or observed experimentally in neat diblock copolymers. Our experimental data are plotted on Milner's morphology diagram in Figure 2.

Based on the TEM image in Figure 3 and the SAXS data in Figure 4, we assign sample I_2S-1 ($\phi_s = 0.89$) a morphology of hexagonally packed PI cylinders in a PS matrix. A linear diblock copolymer of the same composition would form PI spheres in a PS matrix. The observation of optical birefringence in I_2S-1 is consistent with a cylindrical structure. The SAXS pattern contains no preferential orientation of the microphase-separated structure, and thus we display only a one-dimensional

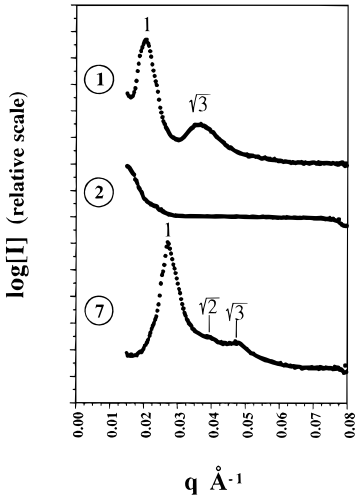

Figure 4. Isotropic SAXS patterns azimuthally integrated into one-dimensional plots of log[intensity] vs q. The intensities are offset for clarity of representation. The circled numbers represent the respective I_2S sample: (1) I_2S-1 ($\phi_s = 0.89$) containing the first two reflections of hexagonally packed cylinders; (2) I_2S-2 ($\phi_s = 0.81$) lacking any discrete interference peaks indicative of the absence of an underlying lattice in the microstructure; (7) I_2S-7 ($\phi_s = 0.09$) containing the first three reflections of a cubic array of spheres.

plot of intensity vs scattering vector, I vs q. We define q^* as the scattering vector of the lowest scattering angle Bragg peak and q_n as the series of Bragg peaks beginning with q^* and including subsequent higher scattering angle peaks. The SAXS pattern for I_2S-1 contains two isotropic rings with q_n/q^* ratios of 1 and $\sqrt{3}$, corresponding to the {10} and {11} sets of planes, respectively, in the hexagonal structure. The TEM images reveal a predominant grain size within the bulk of only several hundred nanometers to a few microns in diameter. The lack of a preferential grain orientation, also evident in the TEM images, is consistent with the isotropic character of the SAXS pattern and the lack of higher order reflections.

The TEM image in Figure 5 and the SAXS pattern in Figure 4 indicate why sample I_2S-2 ($\phi_s = 0.81$) is of particular interest. This sample appears to be microphase separated but not ordered on a lattice. The TEM images indicate a microphase-separated state due to the discrete dark (PI) domains and light (PS) matrix. The pattern of dark dots and short, curved segments is characteristic of a microtomed section through a phase of disordered cylindrical or wormlike micelles.[9] The inset schematic in Figure 5 indicates how a thin section of such a structure produces the resultant image in a 2-D projection. The lack of an underlying lattice is obvious in the micrograph as well as in the lack of any discrete Bragg peaks in the SAXS pattern. Additionally, I_2S-2 displays no optical birefringence, which is consistent with the observation of wormlike micelles distributed isotropically in space.

The lack of any long-range order in this sample immediately made us suspect sample contamination or degradation during the casting and annealing process. However, comparison of GPC traces of the material before casting (as obtained from the original synthesis and purification procedure) and after annealing indicates a pure sample with an extremely narrow molecular weight distribution which undergoes no degradation during sample preparation. The sample casting and annealing procedure for sample I_2S-2 was repeated,

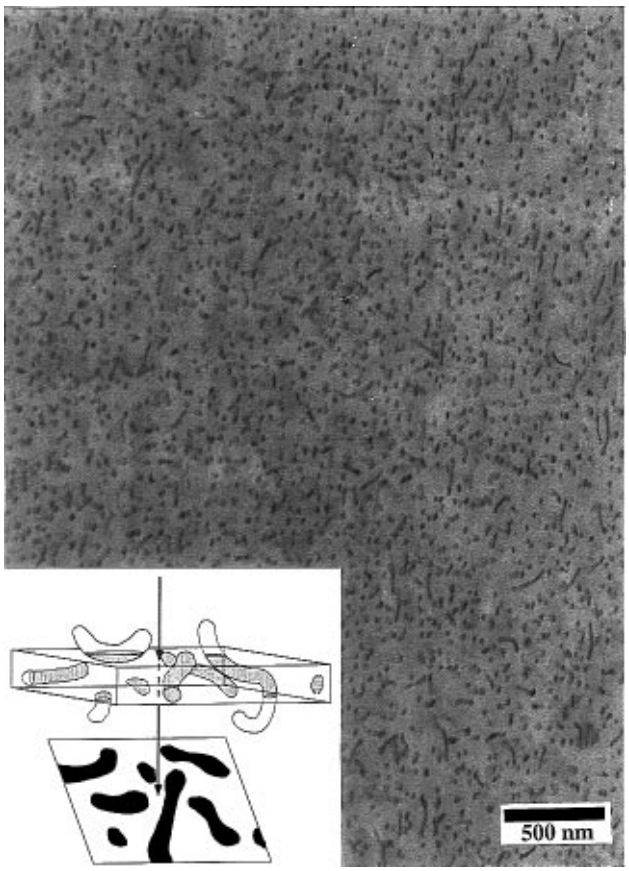

Figure 5. TEM micrograph of I_2S-2 ($\phi_s = 0.81$) showing dark PI wormlike micelles embedded in the PS graft matrix. Inset in the micrograph is a schematic showing how a projection through a microtomed section of the disordered, wormlike micelles appears in a two-dimensional representation as observed in the micrograph.

and the same wormlike micelle morphology was again observed for the neat graft block copolymer. We are thus led to the conclusion that a simple graft block copolymer with the composition of I_2S-2 is unable to form an ordered lattice at this composition. It does, however, microphase separate and display a clear preference for a specific micelle structure. If we look at our series of seven graft copolymers in reverse order (from I_2S-7 to I_2S-1) and compare to Milner's morphology diagram (Figure 2), we see that sample I_2S-2 is the first sample for which the PS graft block is large enough to force the two PI blocks onto the concave side of the interface. This observation is supported by Figure 5 in which it is evident that the PI material (stained to appear dark with OsO_4) is on the concave side of the interface of the microphase-separated, but disordered, domain structures. We hypothesize that frustration inherent in packing the two PI chains on the concave side of the interface inhibits the formation of a morphology with an ordered lattice. However, the reproducible observation of disordered wormlike micelles of constant diameter indicates the approximate selection of a preferred interfacial curvature. Sample I_2S-1, which has even shorter PI chains than I_2S-2, may experience less packing frustration, enabling it to form the hexagonally packed cylindrical structure that we observe. It appears that the inability to form an ordered lattice is confined to a narrow volume fraction range near the transition at which the two PI chains per molecule are initially forced to the concave side of the interface.

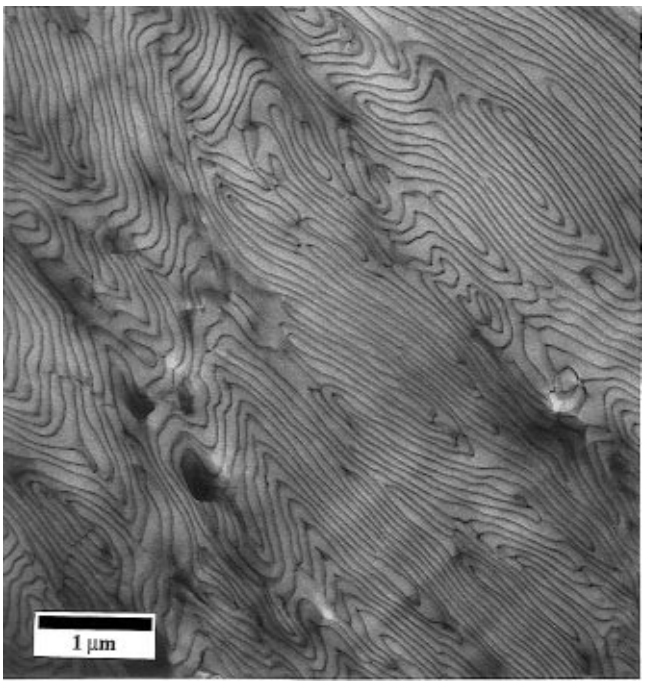

Figure 6. TEM micrograph of I_2S-2 cast from cyclohexane before annealing displaying a kinetically trapped, nonequilibrium lamellar morphology.

If this hypothesis about the lack of long-range order in the I_2S-2 structure is correct, then we should be able to transform this disordered structure into an ordered structure by slightly perturbing the volume fractions in one direction or the other. This can be achieved by casting samples of I_2S-2 from a selective solvent. Casting from cyclohexane, a selective solvent for PI, results in a lamellar morphology as shown in Figure 6. Casting I_2S-2 from dioxane, a selective solvent for PS, enhanced the ability of the single PS graft to force the two PI chains onto the concave side of a highly curved interface, resulting in PI spheres in a PS matrix. After complete removal of the selective solvent, these morphologies are no longer at equilibrium, but are kinetically trapped. Annealing above T_g of the PS block may allow these samples to return to the disordered wormlike micelle structure. Selective solvent casting followed by annealing has been used to demonstrate the equilibrium nature of the structure formed on annealing.[22] Annealing the lamellar interfaces of the cyclohexane cast sample caused them to become perforated in a meshlike morphology[23] which eventually disintegrated back into the disordered wormlike micelle morphology. These selective solvent casting and annealing experiments are described in detail elsewhere.[24]

Sample I_2S-3 ($\phi_s = 0.62$) contains a lamellar microstructure with well-developed, large grains as is evident in the TEM micrograph in Figure 7a. Figure 8a shows an oriented SAXS pattern containing four orders of reflection at q^*, $2q^*$, $3q^*$, and $4q^*$ due to scattering from a cross section of the film placed vertically into the SAXS camera. The concentration of scattered intensity along the equator with arcs extending azimuthally indicates that the lamellar layers are predominantly parallel with the surface of the film. Optical birefringence was observed in sample I_2S-3, consistent with our structural identification of lamella.

Both samples I_2S-4 ($\phi_s = 0.44$) and I_2S-5 ($\phi_s = 0.31$) yield hexagonally packed PS cylinders in a PI matrix and contain regions displaying a remarkable degree of

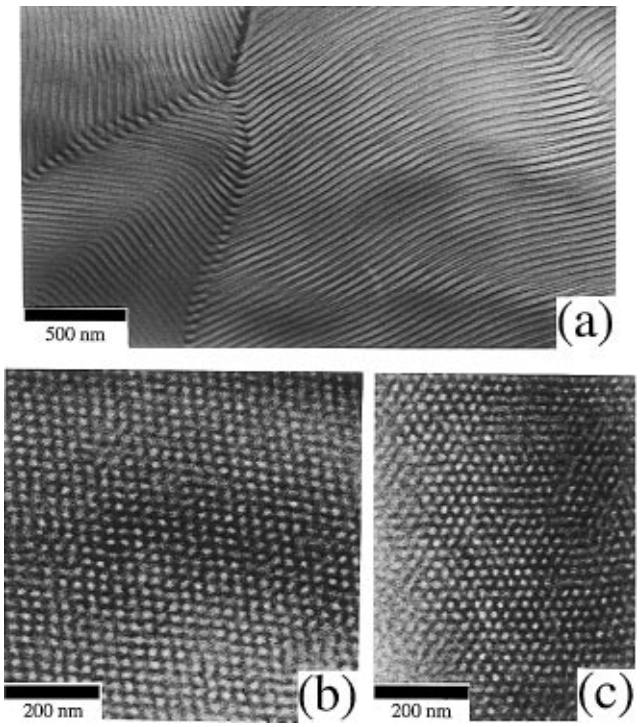

Figure 7. (a) TEM micrograph of I_2S-3 ($\phi_s = 0.62$) showing a lamellar phase. (b) TEM micrograph of I_2S-6 ($\phi_s = 0.17$) showing four-fold symmetry due to a [100] projection of the cubic array of PS spheres. (c) TEM micrograph of I_2S-6 ($\phi_s = 0.17$) containing three-fold hexagonal symmetry due to a [111] projection of the cubic array of spheres.

long-range order, especially considering that no special efforts, such as shearing, were employed to induce alignment. Figures 8b and 8c display two-dimensional SAXS patterns from I_2S-4 and I_2S-5 with sixfold symmetry suggestive of a [001] zone axis of a hexagonally packed array of cylinders. The q_n/q^* ratios of 1, $\sqrt{3}$, $\sqrt{4}$, $\sqrt{7}$, $\sim\sqrt{9}$, and $\sim\sqrt{12}$ correspond to the {10}, {11}, {20}, {21}, {30}, and {22} families of planes, respectively. These hexagonal patterns were taken with X-rays incident through a cross section of the film, indicating that the cylinder axes lie predominantly in the plane of the film. A hexagonally packed cylindrical structure with a remarkable degree of long-range order is clearly evident in TEM micrographs of I_2S-4 and I_2S-5. Figure 9a is a TEM image taken from sections microtomed perpendicular to the surface of the I_2S-4 film. Figure 9b is a projection through a section microtomed parallel with the surface of the same film yielding a projection perpendicular to the cylinder axes which appear as long stripes. SAXS data collected with the sample film surfaces perpendicular to the incident beam produced uniaxial arc patterns with the same q_n/q^* ratio obtained in Figures 8b and 8c indicative of scattering perpendicular to aligned, hexagonally packed cylinder axes. Strong optical birefringence was observed in the sample films, consistent with the assigned cylindrical morphology.

Note the marked difference in degree of long-range order between cylinder-forming samples with PS (graft blocks) forming the cylindrical domains, samples I_2S-4 and I_2S-5, and PI (two chains per molecule) forming the cylindrical domains, sample I_2S-1. We stress that all these samples were cast, annealed, and observed in exactly the same way, so differences in the observed long-range order are not likely to be due to different sample histories. This difference in the quality of long-

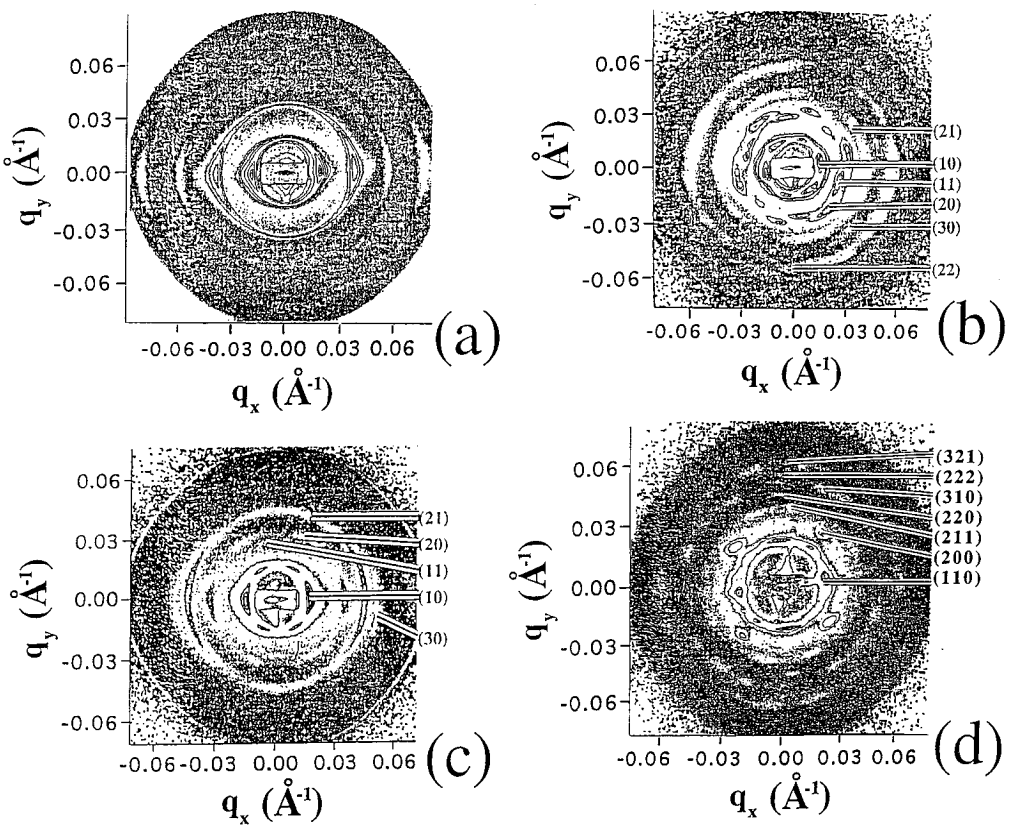

Figure 8. 2-D SAXS data of samples containing a high degree of long-range order of their respective microstructures which produces highly anisotropic scattering patterns. (a) I_2S-3 ($\phi_s = 0.62$) showing the first four orders of the lamellar long period. (b) I_2S-4 ($\phi_s = 0.44$) showing an approximate [001] zone axis of hexagonally packed cylinders (c) I_2S-5 ($\phi_s = 0.36$) also showing the [001] hexagonal zone axis. (d) I_2S-6 ($\phi_s = 0.17$) four-fold symmetry of an approximate [100] zone axis of the bcc array of spheres.

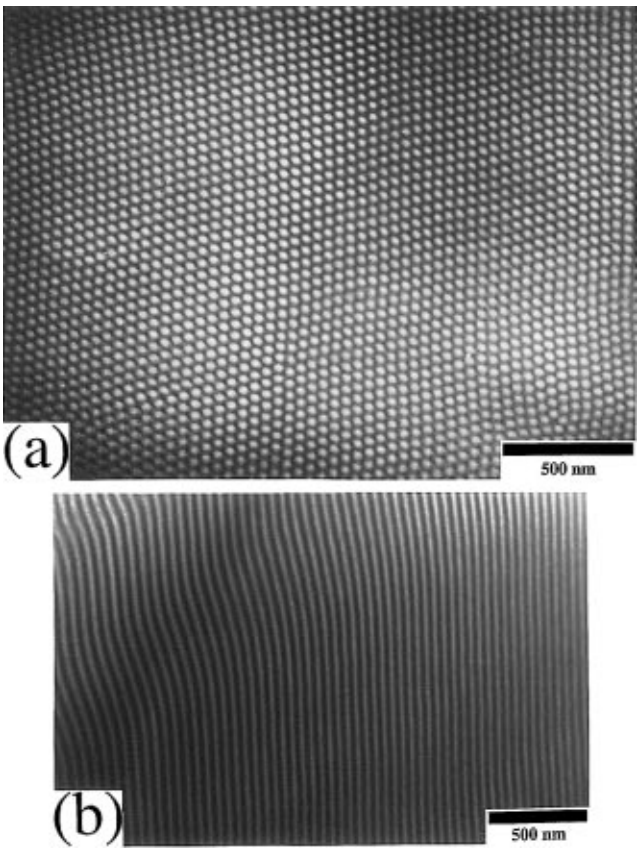

Figure 9. TEM micrographs of I_2S-4 ($\phi_s = 0.44$) (a) taken from sections microtomed perpendicular to the film surface containing an end-on, hexagonal projection of the cylindrical microstructure and (b) taken from sections microtomed parallel with the film surface containing a projection perpendicular to the cylinder axes.

range order for cylinder-forming simple graft samples on opposite sides of the morphology diagram (Figure 2) is a result of the asymmetry in morphological behavior vs volume fraction for ϵ near 2. Samples I_2S-4, I_2S-5, and I_2S-1 all have higher PS volume fractions than linear PS−PI diblocks forming the same type of morphology. In the cases of I_2S-4 and I_2S-5, this results in relatively short PI chains forming the coronas covering the outsides of the PS cylinders. Not only is the PI volume fraction of these corona blocks smaller than the PI volume fraction in a linear PS−PI diblock forming PS cylinders, but the reduced PI volume is divided between two chains per molecule. On the other side of the morphology diagram, the greater volume fraction of the PS graft results in a corona of long PS blocks, much longer than the PS block of a PS−PI diblock of the same molecular weight forming PI cylinders. The packing of the cylindrical micelles onto a hexagonal lattice with long-range order must be controlled by the interaction of neighboring cylinders through their outer, corona blocks. The cylinders in samples I_2S-4 and I_2S-5 interact through coronas of relatively short and highly stretched PI chains. This is a much stiffer and more precise interaction than that between the longer and less stretched PS corona chains in I_2S-1, resulting in greater long-range order for I_2S-4 and I_2S-5.

The simple graft copolymer series is completed by samples I_2S-6 ($\phi_s = 0.17$) and I_2S-7 ($\phi_s = 0.08$), which both formed a cubic array of PS spheres in a matrix of PI. The cast and annealed films displayed no optical birefringence, consistent with a cubic symmetry having no form birefringence. Both the four-fold [100] projection and the hexagonal [111] projection of the I_2S-6 cubic unit cell are shown in Figures 7b and 7c. The TEM images for I_2S-7 are similar. Figure 8d is a SAXS pattern taken from an approximate [100] zone axis of the cubic structure. It displays a characteristic four-fold symmetry of this projection obtained with the surface of the bulk film perpendicular to the X-ray beam. The q_n/q^* ratios of 1, $\sqrt{2}$, $\sqrt{3}$, and $\sqrt{4}$ for the first four reflections are consistent with both body-centered cubic (110, 200, 211, and 220 for bcc) and simple cubic (100, 110, 111, and 200 for sc) symmetries. However, the long-range order is limited due to unavoidable grain boundaries and dislocations, thereby broadening reflections beyond the fourth reflection. The seventh reflection is the first to differ between sc and bcc, producing the 220 at a q_n/q^* of $\sqrt{8}$ for sc and the 321 at q_n/q^* of $\sqrt{7}$ for bcc. To the best of our ability to measure the spacing of the weak seventh reflection, we find a q_n/q^* ratio of approximately $\sqrt{7.3\pm0.4}$, which seems to favor the bcc structure over sc. Chain packing considerations in the Wigner−Seitz cell around each spherical micelle and previous experimental results for linear diblock and starblock copolymers[7,25,26] suggest a bcc packing of spheres as more likely than sc. Sample I_2S-7 did not contain the same degree of long-range order in the spherical microstructure giving rise to the isotropic SAXS pattern displayed in Figure 4.

4. Conclusions

Our experimental results confirm that the architectural asymmetry of the I_2S block copolymers results in a large asymmetry relative to volume fraction in the equilibrium phase behavior. The exact shift from what is found in linear AB diblock materials of the same volume fractions can be directly seen in the phase diagram in Figure 2. The diagram collapses onto the strong segregation phase behavior of conformationally symmetric linear diblocks at $\epsilon = 1$. I_2S-3 and I_2S-7 are the only samples displaying the phase behavior of their diblock analogues, exhibiting lamellar and spherical microstructures, respectively. However, all other samples are shifted into new phase behavior unobtainable for that volume fraction in a diblock architecture. Theoretically, I_2S-2 is shifted from the center of the diblock cylindrical phase very close to the bicontinuous/lamellar phase boundary while experimentally the microstructure is microphase separated into wormlike micelles which are not arranged on a lattice. This microphase-separated but disordered morphology occurs at a composition (81 vol % of the PS graft) which is predicted by Milner's theory to be near the transition to the first structure which requires the two PI chains to be on the concave side of the interface. These results indicate how molecular architecture provides another controllable parameter besides the respective block volume fractions to manipulate the morphology of the bulk.

Acknowledgment. D.J.P. would like to thank G. Dris for help in obtaining GPC traces. J.W.M. and S.P. are grateful to Prof. N. Hadjichristidis for introducing them to well-defined graft copolymers along with discussions and advice throughout. S.P.G., D.J.P., J.W.M., and S.P. would like to acknowledge funding from the U.S. Army Research Office under Contract DAAHO4-94-G-0245. Additionally, S.P.G. acknowledges an Army Young Investigator Award DAAH04-95-I-0305. Central Facility Support from the Materials Research Science and Engineering Center (MRSEC) at the University of

Massachusetts—Amherst and an instrumentation grant from the W.M. Keck Foundation are acknowledged. The authors also acknowledge the synchrotron beam time at Daresbury on EPSRC Grant 26/03 and the technical assistance of Anthony Gleeson.

References and Notes

(1) Hashimoto, T.; Todo, A.; Itoi, H.; Kawai, H. *Macromolecules* **1977**, *10*, 377−384.
(2) Helfand, E.; Wasserman, Z. R. *Macromolecules* **1976**, *9*, 879.
(3) Bates, F. S.; Berney, C. V.; Cohen, R. E. *Macromolecules* **1983**, *16*, 1101.
(4) Winey, K. I.; Thomas, E. L.; Fetters, L. J. *Macromolecules* **1992**, *25*, 2645−2650.
(5) Milner, S. T. *Macromolecules* **1994,** *27*, 2333−2335.
(6) Hadjichristidis, N.; Iatrou, H.; Behal, S. K.; Chludzinski, J. J.; Disko, M. M.; Garner, R. T.; Liang, K. S.; Lohse, D. J.; Milner, S. T. *Macromolecules* **1993,** *26*, 5812−5815.
(7) Olmsted, P. D.; Milner, S. T. *Phys. Rev. Lett.* **1994**, *72*, 936−939.
(8) Milner, S. T.; Witten, T. A.; Cates, M. E. *Macromolecules* **1988**, *21*, 2610.
(9) Kinning, D. J.; Winey, K. I.; Thomas, E. L. *Macromolecules* **1988**, *21*, 3502−3506.
(10) Morton, M.; Fetters, L. J. *Rubber Chem. Technol.* **1975**, *48*, 359.
(11) Roovers, J.; Toporowski, P. *Macromolecules* **1983**, *16*, 843.
(12) Mays, J. W. *Polym. Bull.* **1990**, *23*, 247.
(13) Iatrou, H.; Siakali-Kioulafa, E.; Hadjichristidis, N.; Roovers, J.; Mays, J.W. *J. Polym. Sci., B: Polym. Phys. Ed.* **1995**, *33*, 1925.
(14) *Polymer Handbook*, 3rd ed.; Brandrup, J., Immergut, E. H., Eds.; John Wiley & Sons: New York, 1989.
(15) Floudas, G.; Hadjichristidis, N.; Iatrou, H.; Pakula, T.; Fischer, E. W. *Macromolecules* **1994**, *27*, 7735−7746.
(16) Pispas, S.; Mays, J. W., unpublished data on the glass transition of A_2B copolymers.
(17) Bras, W.; Derbyshire, G. E.; Ryan, A. J.; Mant, G. R.; Felton, R. A.; Lewis, R. A; Hall, C. J.; Greaves, G. N. *Nucl. Instrum. Methods Phys. Res.* **1993**, *A326*, 587.
(18) Lin, C. C.; Jonnalagadda, S. V.; Kesani, P. K.; Dai, H. J.; Balsara, N. P. *Macromolecules* **1994**, *27*, 7769.
(19) Gehlsen, M. D.; Bates, F. S. *Macromolecules* **1994**, *27*, 3611−3618.
(20) Folkes, M. J.; Keller, A. *Polymer* **1971**, *12*, 222.
(21) Balsara, N. P.; Perahia, D.; Safinya, C. R.; Tirrell, M.; Lodge, T. P. *Macromolecules* **1992**, *25*, 3896−3901.
(22) Thomas, E. L.; Alward, D. B.; Kinning, D. J.; Martin, D. C.; Handlin, D. L., Jr.; Fetters, L. J. *Macromolecules* **1986**, *19*, 2197−2202.
(23) Hashimoto, T.; Koizumi, S.; Hasegawa, H.; Izumitani, T.; Hyde, S. T. *Macromolecules* **1992**, *25*, 1433−1439.
(24) Pochan, D. J.; Gido, S. G.; Pispas, S.; Mays, J. W. *Macromolecules*, in press.
(25) Thomas, E. L.; Kinning, D. J.; Alward, D. B.; Henkee, C. S. *Macromolecules* **1987**, *20*, 2934.
(26) Sakurai, S.; Kawada, H.; Hashimoto, T.; Fetters, L. J. *Macromolecules* **1993**, *26*, 5796−5802.
(27) Bates, F. S.; Fredrickson, G. H. *Annu. Rev. Phys. Chem.* **1990**, *41*, 525.

MA951696X